Data Quality for Binary Black Hole Searches with aLIGO

Albert Wandui,[1]
Mentors: Alan Weinstein[2] and Jonah Kanner[2].

[1] *Department of Physics, Stanford University, Stanford, CA 94305*
[2] *The LIGO Project, California Institute of Technology, Pasadena, CA 91125*

(Dated: Sept 25, 2015, DCC Number: LIGO-P1500191)
Key word: LIGO SURF 2015

Abstract

The aLIGO detectors are expected to reach an unprecedented level of sensitivity, which will make direct observations of gravitational waves possible for the very first time. The search for gravitational wave signals, in particular, from the inspiral, merger and ringdown of black hole binaries has been limited by the presence of noise transients called glitches which "trigger" in the gravitational strain channel. We describe a technique for vetoing these glitches by finding correlations between possible glitches in our Binary Black Hole (BBH) Pipeline and noise transients identified in auxiliary channels of the aLIGO instrument. This involves finding the coincidence window between the triggers in the BBH pipeline and triggers in the auxiliary channels that maximizes the efficiency of eliminating glitches from the BBH pipeline and at the same time has a minimal impact on the detector live-time. The goal of this technique is to remove the non-gaussian instrumental transients seen in the gravitational wave strain data which will enable better determination of detection thresholds for actual gravitational wave signals from binary black holes.

Introduction

The aLIGO detectors are expected to reach an unprecedented level of sensitivity. This is likely to make direct gravitational wave observations possible for the first time. Once observation starts, aLIGO expects to see gravitational waves (GWs) from sources such as binary neutron star or black hole systems, galactic core collapse supernovae, asymmetric spinning neutron stars, stochastic sources such as the early universe as well as yet unknown sources of GWs. Such observations will open up the window to the first views of the universe in the gravitational wave spectrum [1].

Even with the high sensitivity of the aLIGO detectors, gravitational wave searches are limited by noise in the detector. The figure (1) shows the dominant noise sources for aLIGO [2]. At low frequencies, quantum fluctuations in the radiation pressure dominate while at high frequencies, quantum shot noise is the main limiting factor.

Data from all the aLIGO detectors show that in addition to the gaussian noise background, which is well understood, there is additional non-gaussian noise fluctuations that produce transient "glitches". These can be mistaken for short duration gravitational wave signals which trigger transient detection pipelines. The distribution of resulting triggers have a tail that stretches to high SNR [3]. Since, in general, the shorter the signal waveform the less capable we are of distinguishing it from the background glitches using signal processing, the non-gaussian short noise transients are a limitation on our ability to effectively detect GW signals from high mass black

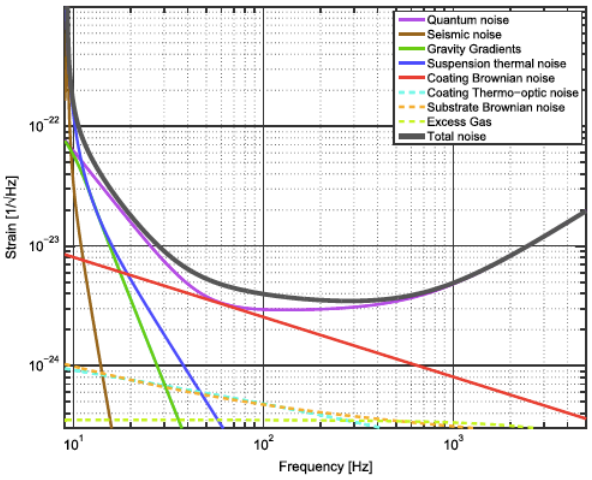

Figure 1: A plot of the dominant noise sources of the aLIGO detector in the frequency domain [2].

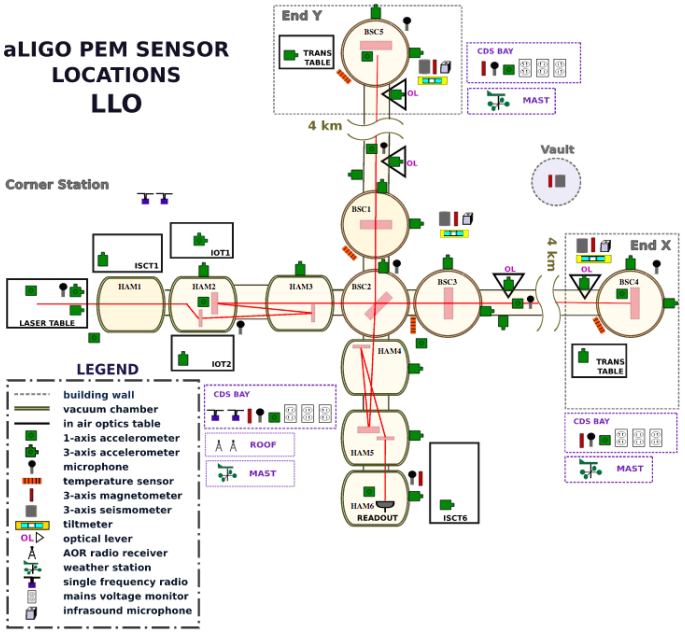

Figure 2: A schematic of the PEM channels currently implemented in the aLIGO instrument at the Livingston site [4].

hole binaries which have very short durations. This necessitates the effort to remove these noise transients by associating them with instrumental glitches witnessed by other channels in the aLIGO detector.

The aLIGO instrument is designed to be isolated from environmental influences and is equipped with sensors that record the state of the local environment. These channels are referred to as the Physical Environment Monitoring (PEM) channels and include seismometers which measure the vibration of the ground, accelerometers that measure the movement of the components of the interferometer, microphones to monitor acoustic noise and magnetometers that record stray magnetic fields that may couple to the test masses or the electronics. Figure (2) shows the location of the different PEM channels currently implemented as part of the aLIGO instrument. Since these PEM channels record environmental influences that may filter into and contaminate the GW data, there is a big effort towards linking transients in these PEM channels to glitches in the BBH pipeline so as to remove the sources of these glitches by improving the instrument, or vetoing sections of the data that are shown to be contaminated.

The internal state of different subsystems of the aLIGO detector is recorded by hundreds of other auxiliary channels that are part of the Interferometer Sensing and Control (ISC) system. Table (1) shows the main aLIGO subsystems that were considered for the purposes of ensuring data quality. Care is taken when selecting candidate channels for use in vetoing triggers derived from the GW strain channel. This is because some channels are closely associated with the GW strain channel and thus may also witness actual GW signals. Such channels are deemed unsafe. Unsafe channels can be identified by the use of high SNR hardware injections during science runs. This involves physically moving the test masses to mimic the action of an incoming GW signal. A channel that is considered safe, shows no response to the injected signal. Figure (3) shows the components for the optical subsystems of the aLIGO detector. It is important to note that the different systems in the aLIGO detector have different characteristic times within which they can affect the GW strain channel. The optical systems, for example are the fastest and thus we expect that glitches in this channels will be almost exactly coincident in time with the glitches that are induced in the GW strain,

$h(t)$, channel. On the other hand, the mechanical systems such as the suspensions, or seismic isolation systems will have a much longer time scale.

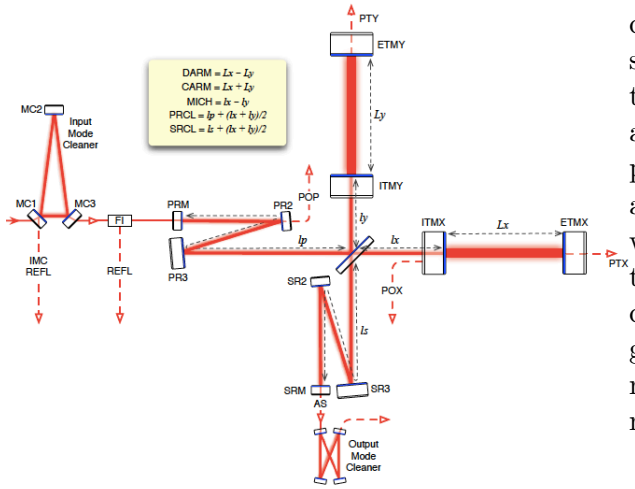

Figure 3: Interferometer optical configuration showing the optical subsystems (ASC, LSC, OMC, IMC) as well as the LSC length degrees-of-freedom. ETMX/Y: End Test Mass X/Y arm; POP: Power Recycling Cavity Pick-off; ITMX/Y: Input Test Mass X/Y arm; REFL: Reflection Port; PRM: Power Recycling Mirror; SRM: Signal Recycling Mirror; AS: Anti-Symmetric Port; PTX/Y: Transmitted Power X/Y arm [5].

Choosing the right channels for the job

Even after eliminating all the channels that are considered unsafe, there are still hundreds of potential auxiliary channels that could be used to veto glitches in the BBH pipeline. Figure (4) shows one such example where glitches in the $h(t)$ channel were coincident with glitches from 2 auxiliary channels: the microphone and a wind monitor. The effectiveness of a given channel in vetoing glitches in the BBH pipeline can be indicated by specifying three indicators: *efficiency*, *deadtime* and the *use percentage* [3].

The efficiency is the fraction of the triggers from the BBH pipeline that are removed by the use of the veto. A key goal of any vetoing strategy is to maximize the efficiency as much as possible. On the other hand, the deadtime is the cumulative observation time that is lost by vetoing corrupted data segments. An effective vetoing strategy only minimally affects the observation time of the detector since this is time in which a GW signal could pass undetected. The use percentage, is the fraction of the triggers of the auxiliary channel that are found to be coincident with triggers in the BBH pipeline. The ratio of the efficiency to the deadtime is a useful indicator of the utility of a channel in vetoing the glitches. A veto with an effiiciency to deadtime ratio that is close to one, is simply no better than removing data segments at random.

The most useful channels for the veto were selected using an algorithm called Hveto [3]. Hveto analyzes hundreds of channels and ranks the channels based on a statistical significance measure that quantifies how unlikely it is to see that number of coincidences between the auxiliary channel and the BBH pipeline as compared to a random Poisson process. The advantage of using Hveto is its hierarchical nature; by analyzing the channels in stages, it determines the best available channel at that particular stage. All the coincident glitches are removed at each stage to ensure no redundancy and the process is iterated. In this analysis, the 18 most significant channels as determined by Hveto were used to create the veto.

It is difficult to determine which parameters the efficiency and deadtime depend upon. This is because different channels have a wide range of amplitudes and may have short time offsets between the disturbances in the auxiliary channels and the $h(t)$ channel. This research focused on testing the size of the coincidence window and the SNR threshold as the main parameters of the veto. Our tests were done using all the clustered BBH triggers from the ER7 run. For all the triggers in the BBH pipeline, the offsets from the Omicron triggers were computed and plotted as a histogram. Omicron is a simple glitch finding "Event Trigger Generator" (ETG) that is computationally efficient, so that it can be run on

Subsystem	*Brief Description*
Length Sensing & Control (LSC)	Maintains optical resonance in the interferometer. Also provides the Gravitational Wave readout from the Differential Mode of the detector (DARM) as well as the Common Mode (CARM).
Alignment Sensing & Control (ASC)	Checks and maintains the angular motion of the optical system.
Signal Recycling Cavity (SRC)	Located at the antisymmetric output of the detector. Lowers arm cavity finesse for GW signals so as to maintain a broadband detector frequency response.
Power Recycling Cavity (PRC)	Resonant cavity between the laser input and the Michelson interferometer. Increases the effective power of the laser beam.
Output Mode Cleaner (OMC)	Positioned between the AntiSymmetric (AS) Port and the DC readout photodiodes for sensing the DARM. Filters out the higher order spatial modes and the RF sidebands on the laser light, passing only the fundamental DC carrier mode and the audio frequency (GW signal) sidebands.
Input Mode Cleaner (IMC)	Stabilizes the beam in position and provides a high quality laser frequency reference.
Suspensions (SUS)	Pendulum systems that provide passive isolation from ground motion and thermal noise.
Seismic Isolation System (SEI)	Provides active isolation of the detector components from ground motion.
Physical Environment Monitoring (PEM)	Sensors that record the state of the local environment.

Table 1: Key subsystems in aLIGO and their descriptions. All the channels used in the vetoing process were from these subsystems [2, 5].

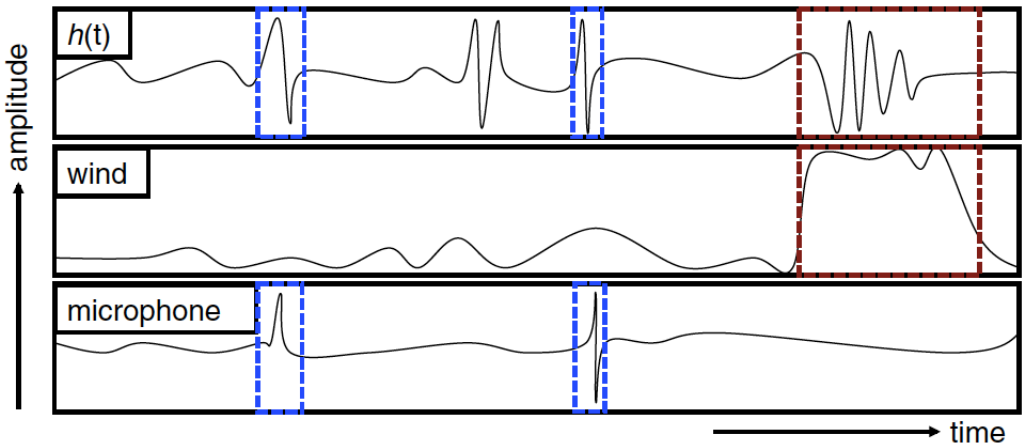

Figure 4: An illustration of the removal of glitches in the $h(t)$ channel due to their correlation which transients in two auxiliary channels [3].

very many auxiliary channels (as well as the h(t) channel). It produced list of glitch triggers from each channel. Omicron is described in more detail in Appendix 2[6]. If an auxiliary channel is completely uncorrelated with the $h(t)$ channel, only a flat accidental background rate would be seen in the histogram. Any trigger from the auxiliary channel would have an equal probability of being found at a given offset from a BBH trigger. Instead, we found a large peak centered at a zero offset as clear indicator of a correlation. The peak decays over several seconds into a background accidental coincidence rate as can be seen in figure (5). Offsets can be positive or negative. A negative offset, implies that the peak time of the Omicron trigger happened before the end time of the corresponding BBH trigger. The coincidence window is then chosen to eliminate the BBH triggers in this peak. The two vertical lines in the figure indicate the size of the coincidence window that was chosen so as to eliminate most of the BBH triggers in the peak.

For all the channels, the size of the coincidence window was determined and fixed and the SNR threshold on the triggers from the auxiliary channel was varied as the free parameter. Multiple values of the SNR threshold were tested and the efficiency vs deadtime determined and plotted in a receiver operator curve (ROC) to determine the operating point of the veto. This is the point closest to the left hand corner of the ROC curve. Figure (6) shows an ROC curve for Hveto. The high efficiency at very low deadtime costs shows the utility of the vetoing strategy.

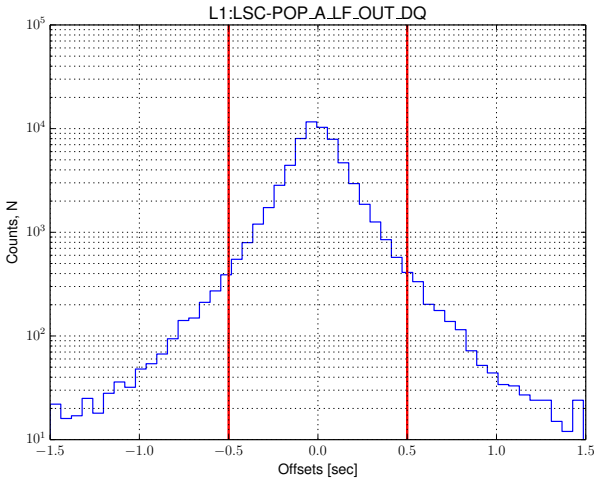

Figure 5: Histogram showing the offset between BBH triggers and triggers from the channel L1:LSC-POP_A_LF_OUT_DQ. This channel is records signals from the Pick-Off Port of the Power Recycling Cavity. The peak centered at a zero offset shows that there is a non-trivial correlation between the two channels. The two red lines indicate the size of the coincidence window chosen to be symmetric about the peak. All BBH triggers within the coincidence window were vetoed.

Results and Discussion

For each channel being considered, a one second coincidence window was set and the SNR threshold which gave the highest efficiency to deadtime ratio was determined. The results for 4 such channels are shown in the table (2). The table also shows that despite having widely varying SNR thresholds, all the channels registered similar ratios of efficiency to the deadtime. Whether this is as a result of coincidence or signals some deeper underlying reason is still unknown and is currently being investigated.

When the efficiency is plotted against the deadtime, the dependence of the veto performance on SNR threshold is made even more explicit. From figure(7) At low SNR Thresholds, the vetoing efficiency is very high but at a correspondingly large deadtime cost. Similarly, when the SNR threshold is raised too high, the efficiency drops significantly, making the veto ineffective.

The high deadtime costs are a barrier to the practical implementation of this veto in the data analysis. However, a further study of the relationship between the triggers that were vetoed and the triggers in the auxiliary channel may be beneficial in further constraining the veto so as to cut the deadtime costs. One such example of this is the L1:LSC-POP_A_LF_OUT_DQ channel which records low frequency power from the

Channel	SNR Threshold ρ^*	Efficiency/ Deadtime
ASC-AS_B_RF36_I_YAW_OUT_DQ	40	2.2690
LSC-POP_A_LF_OUT_DQ	100	2.3015
PEM-EX_TILT_VEA_FLOOR_T_DQ	40	2.3538
SUS-OMC_M1_ISIWIT_T_DQ	12	2.3804

Table 2: Several LIGO auxiliary channels and their performance in the veto.

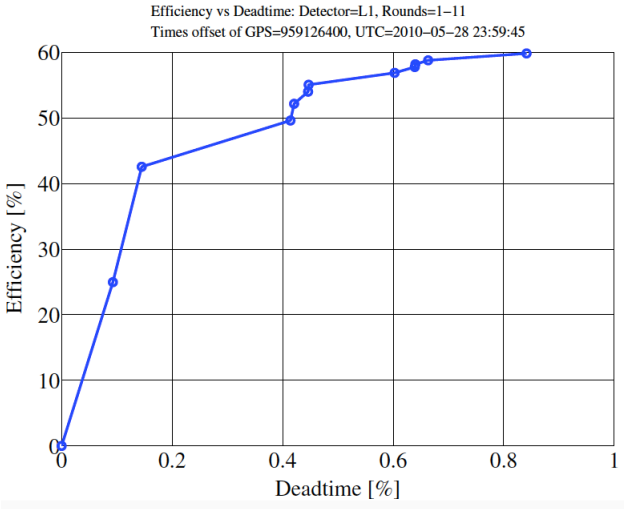

Figure 6: ROC curve for Hveto during the first 11 rounds of vetoing. Here, the SNR threshold of the auxiliary channel Omicron triggers is being varied. Lower SNR thresholds give higher veto efficiency but also higher deadtime. The high efficiency of Hveto with very low deadtime costs shows that it is a very effective vetoing algorithm [3].

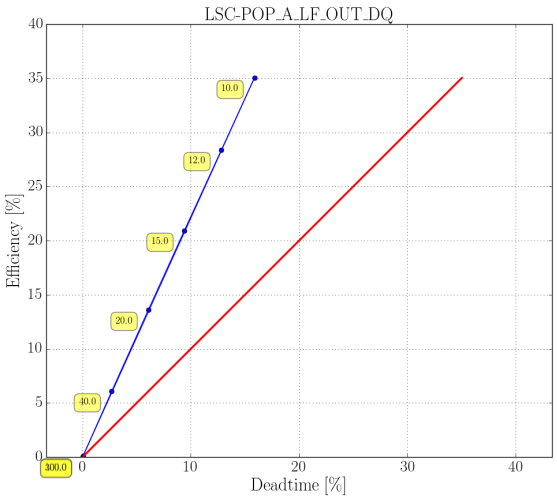

Figure 7: The efficiency vs deadtime plot for one of the channels being considered. The red curve shows the characteristic of a purely random veto. The blue curve shows the correlation between the triggers in the auxiliary channel and the BBH pipeline. For each point on the plot,the corresponding SNR Threshold is also indicated.

pick-off port of the power recycling cavity. A plot of the SNR vs the central frequency of all the triggers in the channel reveals a low SNR background at all frequencies. Superimposed on this background is a rising peak centered at about 500 Hz that rises to very high SNR. This can be seen in figure(8). This plot makes clear the behavior seen in the ROC plot. It is a fair assumption that the noise transients about the peak are responsible for the glitches in the $h(t)$ channel. Thus raising the SNR threshold isolates these particular triggers from the much larger background that extends over all frequencies. For such a channel, the veto could be further refined by only using triggers with a frequency close to 500 Hz to construct the coincidence window and implement the veto. Such a study also sheds light on the characteristics of the noise in this particular channel and is useful to the detchar group that aims to identify and remove such noise sources [6]. It should be noted that not all channels that were considered in this study displayed such clear frequency dependence.

This study also revealed that the SNR of triggers in the BBH pipeline did not relate directly to the SNR of the triggers in the auxiliary channels. Even though a threshold was set on the

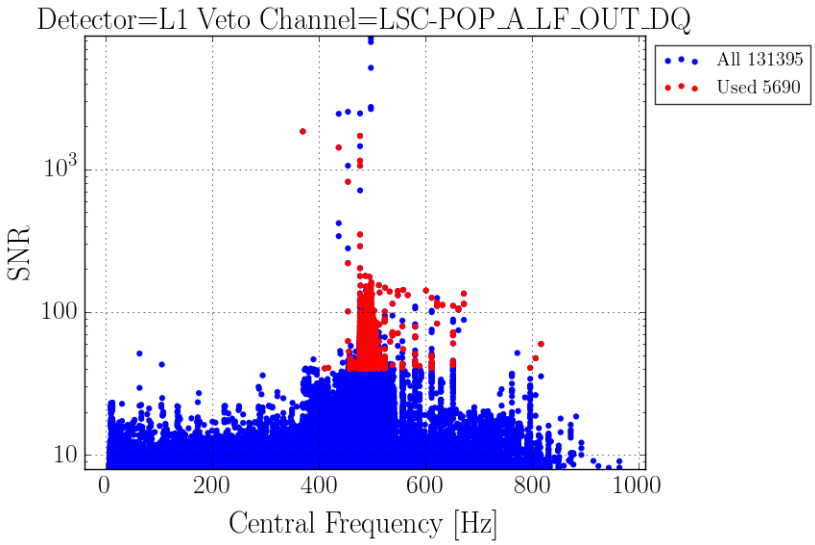

Figure 8: A SNR vs central frequency plot of the L1:LSC-POP_A_LF_OUT_DQ channel. Note the rising peak at around 500 Hz. The red markers indicate all the triggers that were found to be coincident with BBH triggers in a veto with an SNR threshold of 40.

triggers in the auxiliary channel, this did not lead to a preferential elimination of triggers above a certain SNR in the BBH pipeline. In fact, many of the channels considered eliminated triggers in the BBH pipeline at all SNR values. An example of this can be seen in the histogram (9) which shows the efficiency of the of the L1:LSC-POP_A_LF_OUT_DQ channel discussed above in vetoing BBH triggers when the SNR threshold was set at 40.

The particular characteristic of the triggers in the BBH pipeline that is best correlated with the triggers from the auxiliary channel that are used in the veto is yet to be determined. A likely candidate might be the chirp mass $\mathcal{M}$. This is because the triggers from some of the auxiliary channels have shown a strong frequency dependence. The central frequency and the quality factor determine the duration of the trigger in the auxiliary channel as is discussed in Appendix 2. The chirp mass on the other hand, can be used as an indicator of the duration of the trigger in the BBH pipeline because high chirp mass signals have shorter durations. Since the chirp mass and the central frequency are both indicators of trigger duration they may be correlated. However, such a relationship is yet to be demonstrated. If such a relationship is determined, triggers in the BBH pipeline that fit the desired characteristics could be more easily eliminated improving the sensitivity of the detector to true gravitational signals.

Summary

Through this project, we were able to undertake crucial steps in designing a new veto for triggers in the BBH pipeline. We identified suitable and safe auxiliary channels for use in constructing the veto using the Hveto algorithm. Hveto analyzes channels based on a significance criteria. Due to its hierarchical nature, we were able to identify 18 channels that targeted different glitches in the BBH pipeline and thus eliminating redundancy of the veto. Once the channels to use for the veto were determined, we settled on a set of three veto performance criteria: efficiency, deadtime and the use percentage. The efficiency was a measure of how many triggers in the BBH pipeline could be eliminated by the use of the veto. The deadtime was defined as the fraction of observation time we lost when we vetoed a set of triggers from the BBH pipeline. The use percentage on the other hand, is a measure only

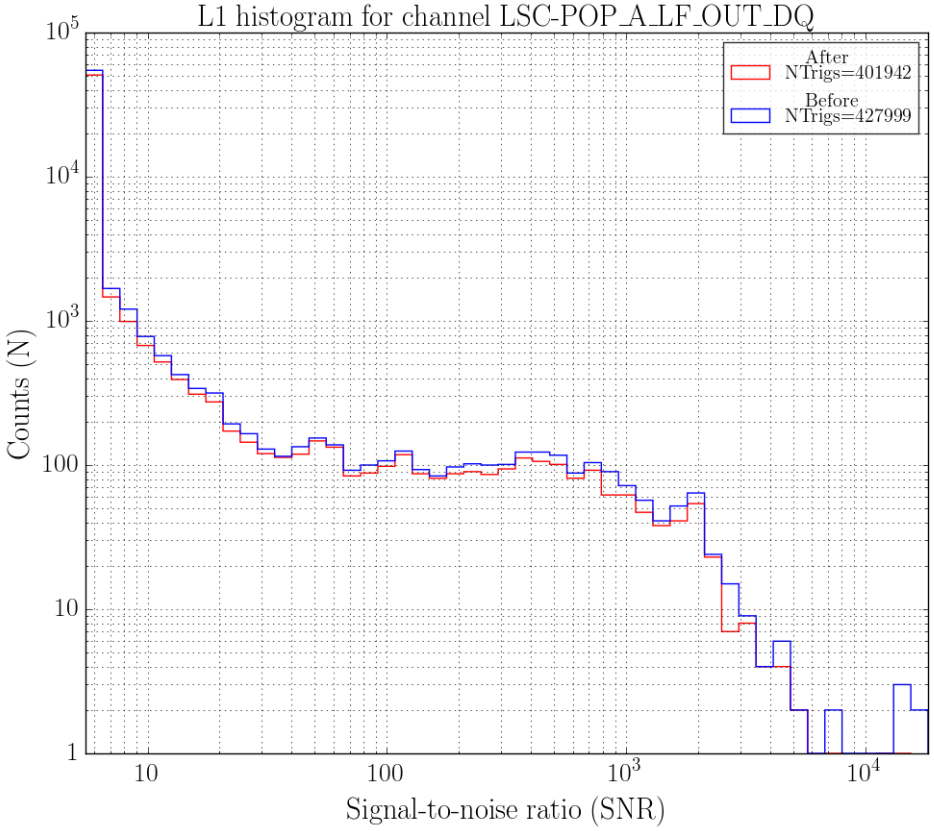

Figure 9: Histogram showing the number of triggers left in the $h(t)$ channel both before and after the vetoing of triggers coincident with triggers of the L1:LSC-POP_A_LF_OUT_DQ channel. The SNR threshold for the auxiliary triggers was set at 40 in this case. Note that triggers at all SNR are found to be coincident with triggers from the auxiliary channel.

of the performance of the auxiliary channel. It is the number of triggers is the auxiliary channel that were found to be coincident with BBH triggers.

The bulk of the research however, was in determining the size of the coincidence window as well as the SNR threshold for which veto performance could be maximized. Our goal was to determine the values of these parameters for which the efficiency would be maximized and deadtime minimized and use that as the operational point of the veto. For this research, we fixed the size of the coincidence window and varied the SNR threshold freely so as to step through the parameter space. The results were then presented as an ROC curve showing how efficiency and deadtime changed as a function of the SNR threshold. As expected, for low SNR thresholds, we saw very high vetoing efficiency but at unacceptably high deadtime costs.

In order to better understand the coincidence between the triggers in the auxiliary channel and the BBH pipeline, we similarly investigated the trigger characteristics of the coincident triggers. For triggers in the BBH pipeline, the key characteristic that was investigated was the SNR. For triggers in the auxiliary channel, we analyzed both the central frequency and SNR of the triggers. In one of the channels considered for example: L1:LSC-POP_A_LF_OUT_DQ, we identified a broad loud peak in the central frequency at about 500Hz which we showed to be responsible for the coincident triggers (8).

Conclusion

In conclusion, we determined there was a significant correlation between the triggers in the BBH pipeline and those from the auxiliary channel. The efficiency and deadtime could be suitably parametrized by the SNR threshold that is set on the triggers from the auxiliary channel. With a low SNR threshold, we achieved high vetoing efficiency as well as high deadtime costs. As the SNR threshold is raised, the deadtime cost is reduced but the efficiency drops as well. With our current choice of 1 second long coincidence windows, the deadtime costs are too high for the practical use of veto.

Even so, we showed that information from these first runs could be fed back into the process of determining the best parameters to use for the veto. As a result of analyzing the relationship between the vetoed triggers in the BBH pipeline and the triggers from the auxiliary channel used in the veto, we were able to demonstrate that other characteristics of the triggers such as the central frequency, may play a crucial role in determining which triggers are actually coincident. We also showed that there was no clear relationship between the SNR threshold used in the veto and the SNR of the vetoed BBH triggers.

Future Work

The next steps in this project involve making the coincident window a free parameter as well. In this project, we assumed that all the channels would have the same coincidence window which we fixed at 1 second. Changing the size of the coincidence window will allow the veto to be more selective in targeting triggers in the BBH pipeline. The relationship between the coincidence times and the triggers that were found to be coincident is still an open question. It has not been demonstrated if within that chosen 1 second window, the vetoed triggers are found within a smaller time interval or distributed over all times. If such a relationship can be determined, then the coincidence window can be determined with better accuracy leading to lower deadtime costs of the veto.

In addition, this research is useful for detector characterization. If a relationship between the vetoed triggers in the BBH pipeline and the triggers in the auxiliary channel can be demonstrated for each channel being used in the veto, we can better understand which physical mechanisms of the aLIGO detector are responsible for the noise processes. This will also allow us to better constrain the veto to only target the triggers for which the relationship can be demonstrated as being likely glitch candidates. With this steps, we will be able to create a high precision veto with low deadtime costs for the BBH pipeline. The improvement in the data quality that this will allow will allow us to detect gravitational wave signals from binary black holes at a higher significance.

Acknowledgement

I would like to thank Prof. Alan Weinstein, Jonah Kanner, Tjonnie Li and Jess McIver for their mentorship in the shaping and implementation of this project. I would also like to gratefully acknowledge the LIGO Laboratory and the National Science Fund NSF for their funding support without which I could not conduct this research.

Appendix 1: GWs from Binary Black Hole Inspirals

GWs have very small amplitudes which makes observing them very difficult. These amplitudes have been calculated not by solving the full Einstein's equations but rather from approximations and numerical solutions. The quadrupole approximation is very useful in understanding GWs emitted by gravitationally bound systems, many of which are the target of aLIGO. In this scheme, the dominant term in the generation of gravitational waves is the second derivative of the second moment of the mass distribution of the source. For example, for a binary neutron star system with a quadrupole moments $I_{\mu\nu}$, an orbital frequency f, orbital radius R, total mass

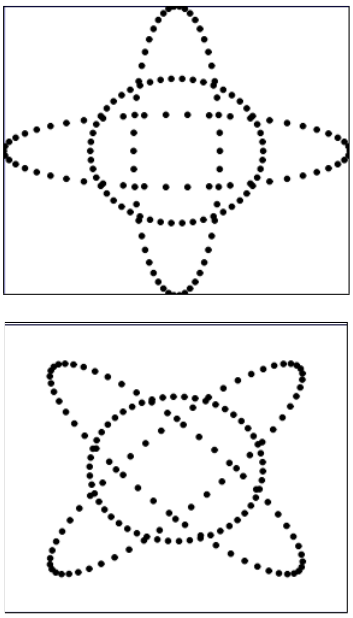

Figure 10: The purely plus and purely cross polarization states of gravitational waves on the top and bottom panels respectively. The two polarization states have an angle of $\pi/4$ between them [7].

M and at a distance r from us, we can use dimensional analysis to predict the amplitude of the gravitational wave.

$$h_{\mu\nu} = \frac{2G}{c^4 r}\ddot{I}_{\mu\nu} \implies h \approx \frac{4\pi^2 GMR^2 f^2}{c^4 r} \tag{1}$$

which gives GW strains of the order of 10^{-21}!

In General Relativity, gravitational waves are represented by a second rank tensor [1]. They carry energy and momentum away from their sources and travel at the speed of light. These GWs cause miniscule tidal deformations when passing. Similarly to electromagnetism, there are 2 independent polarizations, the plus and the cross, duly named after the effect that they produce on such a ring of particles. A key difference, is that the angle between the two polarization states is $\pi/4$ whereas in electromagnetism it is $\pi/2$. Figure (10) shows how the circular ring of particles is deformed into ellipses of the same area. Note the difference in the effects of the plus versus the cross polarizations.

In the quadrupole approximation, the two polarizations take the following form far from the source during the inspiral phase up to the coalescence time t_c [8]

$$h_+(t) = -\frac{2G\mathcal{M}}{c^2 D}\frac{(1+cos^2\ \iota)}{2}\left(\frac{c^3(t_c-t)}{5G\mathcal{M}}\right)^{-1/4} \times cos\left[2\Phi_c - 2\left(\frac{c^3(t_c-t)}{5G\mathcal{M}}\right)\right]$$

$$h_\times(t) = \frac{2G\mathcal{M}}{c^2 D}cos\ \iota\left(\frac{c^3(t_c-t)}{5G\mathcal{M}}\right)^{-1/4} \times sin\left[2\Phi_c - 2\left(\frac{c^3(t_c-t)}{5G\mathcal{M}}\right)\right]. \tag{2}$$

D is the distance to the binary system, $\mathcal{M}$ is the chirp mass defined as $\mu^{3/5}M^{2/5} = \eta^{3/5}M$ where $\mu = \frac{m_1 m_2}{m_1+m_2}$ is the reduced mass, $M = m_1 + m_2$ is the total mass and $\eta = \mu/M$ is the symmetric mass ratio. Φ is the orbital phase of the system with Φ_c being the orbital phase at coalescence. In the fourier space, we can obtain suitable waveforms by taking the fourier transform of the time domain waveforms in equation (2). However, analytical expressions can be obtained using the stationary phase approximation. In the inspiral, the strain in the frequency domain is proportional to $f^{-7/6}$

$$\tilde{h}(f) = \mathcal{A}f^{-7/6}e^{-i\Psi(f)}. \tag{3}$$

Here, $\mathcal{A}$ is a constant and $\Psi(f)$ is the phase evolution. From the above equations, we see that as the orbit of the system decays, both the frequency and the amplitude of the GWs emitted increases. This is the typical chirp of the inspiral of binary compact objects (neutron stars and black holes). Figures (11a, 11b) show the dependence of the shape of the gravitational waveforms in frequency space and in time respectively, as the total mass of the system is varied. With higher chirp masses, we have shorter duration waveforms. Figure(12a, 12b) show how the frequency characteristic and profile of the waveforms change when spin is introduced. Here, the spins are antiparallel and are pointing out of the plane of the orbit. Both binary blackholes in these system are equal mass. The different waveforms shown, correspond to the different

approximations used to describe compact binary coalescence with spin.

The inclination angle of the system with respect to the observer, ι determines the polarization [7]. When the system is seen edge on, the GW is plus polarized while when the orbit is face on, the GW has equal plus and cross polarizations and is said to be circularly polarized. Since the inclination is usually not known during observation, it and other contributions due to the antenna response function are usually absorbed into the distance giving an effective distance, D_{eff} to the binary system. Closer to the moment of coalescence and during the merger and later ringdown, higher order terms in the the expressions for the strains must be added since the system becomes highly relativistic in the strong gravitational field regime. Here, numerical relativity can be used to solve the full Einstein equations and produce waveforms both with and without spin. The presence of aligned or non-aligned spin alters the waveforms in this later stages and the waveforms become even more complex when the spins are precessing.

Different passing GWs will cause differential strains on the two arms of aLIGO interferometer which can be measured as a path difference between the two laser beams in the arms when they interfere at the beam splitter [2]. We therefore can measure, the induced strain, $h(t)$ in the gravitational wave channel, which is a function of the polarization.

$$h(t) = F_+ h_+(t) + F_\times h_\times(t) \qquad (4)$$

where F_+ and $F_\times$ are the antenna response functions of the detector. The antenna response functions depend on the location of the source with respect to the detector and they change with time since the earth is rotating with respect to the celestial sphere. Figure (13) shows the r.m.s response of the antenna to incoming GWs. GWs coming from sources in the plane of a detector, at exactly 45 deg angle are undetected, while the detectors are most sensitive to GWs from sources directly overhead. The aLIGO detectors can also be seen to be approximately omnidirectional.

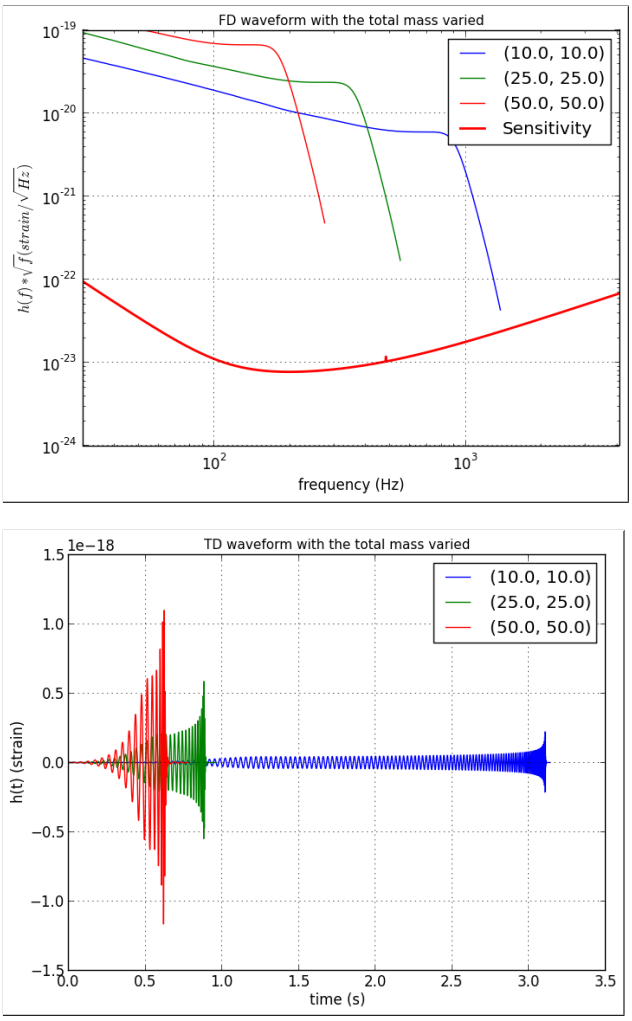

Figure 11: Plots showing the shape of the waveforms in the frequency domain (upper) and time domain (lower) as the total mass M is varied with the mass ratio kept constant and no spins. In the FD, the first part of the wave is seen to be proportional to $f^{-7/6}$ and is the inspiral phase. The merger and the subsequent ringdown in the TD can be seen as the amplitude of the wave rises and then drops sharply over a few cycles. As M increases,the amplitude of the strain increases and the waveform lasts for a shorter period. The lower solid red curve in the upper plot is the sensitivity of aLIGO to GW strains. For all three waveforms all three stages: inspiral, merger and ringdown would be detectable by aLIGO.

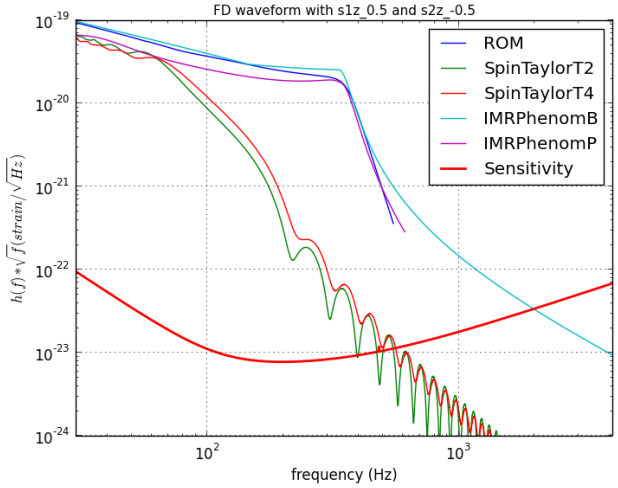

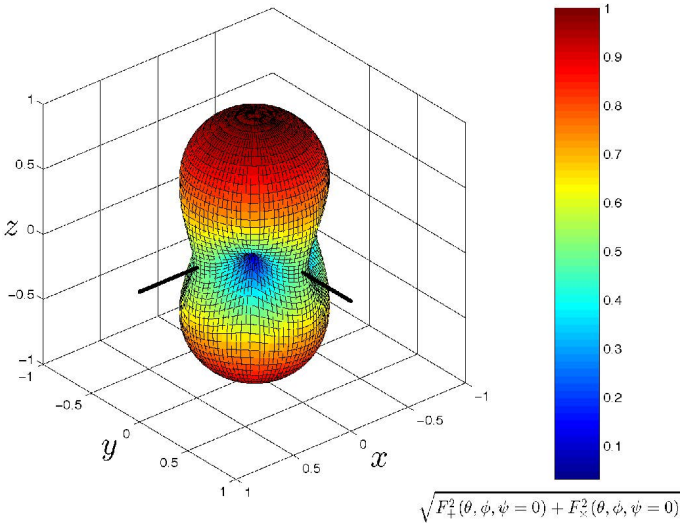

Figure 13: The r.m.s unpolarized antenna response of the aLIGO detector. The black arms X and Y arms represent the two arms of the detector [7].

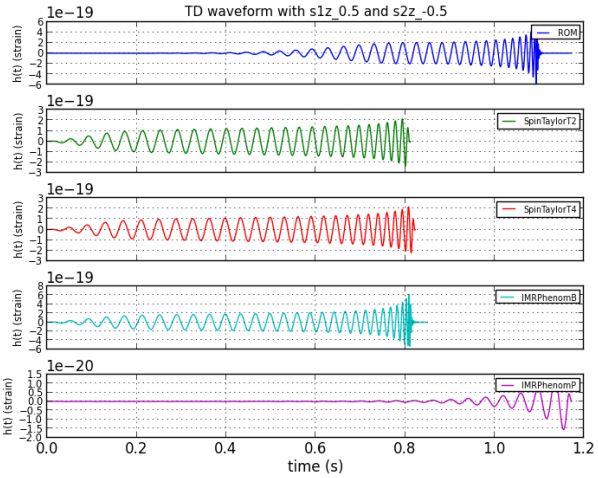

Figure 12: Plots showing GWs under different approximations and with precessing spins. The waveforms show much more complexity such as the amplitude not increasing monotonically with time. These features arise due to spin-orbit coupling which causes the orbit to precess over time, changing the polarization of the GWs.

Appendix 2: Obtaining noise transients from auxiliary channels

Because glitches in the auxiliary channels are generally unmodelled waveforms, the matched filtering strategy applied to the BBH pipeline fails. Instead, Omicron, which is the Event Trigger Generator (ETG) for glitches in the auxiliary channels, searches for the excess power of the burst and uses that information to characterize the transients. Using Omicron, we can recover the energy, time, central frequency, bandwidth, duration and the SNR of the noise transient. This is done by expressing the glitch waveform in a basis defined by a choice of a normalized wavefunction $\Psi(t)$. Using this basis, we can express the glitch signal $g(t)$ as:

$$g(t) = |g|\Psi(t) \text{ where} \tag{5}$$

$$|g|^2 = \int_{-\infty}^{\infty} |g(t)|^2 \mathrm{d}t \tag{6}$$

$$= \int_{-\infty}^{\infty} |\tilde{g}(f)|^2 \mathrm{d}f \tag{7}$$

and $\tilde{g}(f)$ is the fourier transform of $g(t)$. Using the wavefunction basis, we can now define the time of the transient as

$$t_0 = \int_{-\infty}^{\infty} t|\Psi(t)|^2 \mathrm{d}t. \tag{8}$$

Similarly, the central frequency of the transient is defined using the Fourier transform of the wavefunction:

$$f_0 = \int_{-\infty}^{\infty} f|\tilde{\Psi}(f)|^2 \mathrm{d}f. \tag{9}$$

The variance in the time and the frequency domain will define the duration and the bandwidth of the transient respectively.

$$\sigma_t^2 = \int_{-\infty}^{\infty} (t - t_0)^2 |\Psi(t)|^2 \mathrm{d}t \tag{10}$$

$$\sigma_f^2 = \int_{-\infty}^{\infty} (f - f_0)^2 |\tilde{\Psi}(f)|^2 \mathrm{d}f. \tag{11}$$

It is also convenient to define a quality factor, Q defined by the relation $Q = f_0/\sigma_f$. Thus by specifying $t_0, f_0, \sigma_t, \sigma_f, Q$ and the SNR ρ, we can uniquely characterize a noise transient. In order to then recover the excess power, the data are projected onto a time-frequency plane that is determined by the choice of the wavefunction basis. For noise transients, since we assume that they are all short duration and narrow band, the sine-gaussian is a convenient basis with which to map the data. Figure (14) shows an example of a sine-gaussian waveform. For a sine-gaussian, Q will determine the number of oscillations before the waveform dies down to $1/e$ of its peak value.

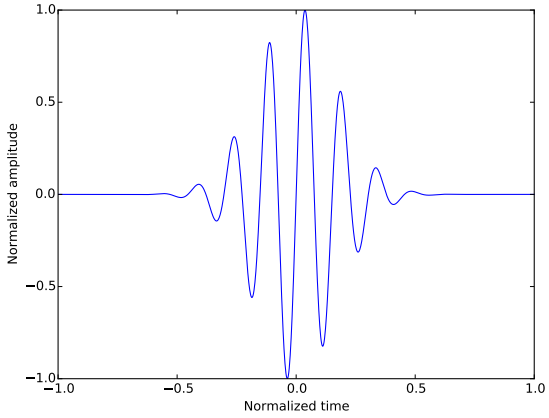

Figure 14: A sine gaussian signal in the time domain parametrized by Q = 10 and f_0 = 1 Hz .

The uncertainty relation between σ_t and σ_f means that better resolution in time is at the expense of resolution in frequency and vice versa. However, the choice of sine-gaussians as the basis is advantageous since it gives us the minimum relation in the uncertainty principle:

$$\sigma_t \sigma_f = \frac{1}{4\pi}. \tag{12}$$

To optimize the placement of the discrete tiles in the time-frequency plane, Q bridges the resolution between the spacing in time Δt vs spacing in frequency Δf. From the uncertainty principle we can conclude that:

$$Q = \frac{f_0}{\Delta f} = 4\pi f_0 \Delta t. \tag{13}$$

This enables us to construct multiple time-frequency maps by fixing the value of Q for a particular map and using it to govern the spacing in time Δt because as we increase the central frequency, the duration of our sine-gaussian signal decreases. In Omicron, the spacing is chosen to be linear in time and logarithmic in both the central frequency and in the spacing of the Q planes. Now, we can define the excess power Z_j in tile j given the amplitude of the tile, $|X_j|$and use it to construct an SNR for our noise transient by the relation

$$Z = \frac{|X_j|^2}{\langle |X|^2 \rangle} - 1 \tag{14}$$

where $\langle |X|^2 \rangle$ is the mean energy of the tiles at that central frequency. This is an estimate of the tile energies in the absence of a non-Gaussian glitch. We can then set a threshold on Z to identify our glitches. However, since loud glitches will usually generate many events that are closely spaced in both time and frequency, the triggers generated are usually clustered and the highest Z is chosen. We can then estimate the SNR of the trigger contained in one tile $\rho_{tile} = \sqrt{Z}$.

References

[1] B.S Sathyaprakash and F. Schutz Bernard. Physics, Astrophysics and Cosmology with Gravitational Waves. *Living Reviews in Relativity*, 2009.

[2] The LIGO Scientific Collaboration, J Aasi, B P Abbott, R Abbott, T Abbott, M R Abernathy, K Ackley, C, and et al. Advanced ligo. *Classical and Quantum Gravity*, 32(7):074001, 2015.

[3] J.R Smith, T Abbott, E Hirose, N Leroy, D MacLeod, J McIver, P Saulson, and P Shawhan. A hierarchical method for vetoing noise transients in gravitational-wave detectors. *Classical and Quantum Gravity*, 28(23):235005, 2011.

[4] M Tse, V Roma, and T Hardwick. Pem channel info, 2015. [Online; accessed 29-July-2015].

[5] Rich Abbott, Rana Adhikari, Stefan Ballmer, Lisa Barsotti, Matt Evans, Peter Fritschel, Valera Frolov, Guido Mueller, Bram Slagmolen, and Sam Waldman. Advanced LIGO length sensing and control final design. 2010.

[6] Hunter Gabbard. Characterization of the Omicron Trigger Generator and Transient Analysis of aLIGO Data. *IREU Final Report*, August 2014.

[7] Kari Hodge. The search for gravitational waves from the coalescence of black hole binary systems in data from the LIGO and Virgo detectors. Or: A dark walk through a random forest. 2014.

[8] B. Allen, W. G. Anderson, P. R. Brady, D. A. Brown, and J. D. E. Creighton. FINDCHIRP: An algorithm for detection of gravitational waves from inspiraling compact binaries. 2012.